Analysis of surface acoustic wave induced spin resonance of a spin accumulation

R. Jansen,[1] P. Dhagat,[2] A. Spiesser,[1] H. Saito,[1] and S. Yuasa[1]

[1]*Spintronics Research Center, National Institute of Advanced Industrial Science and Technology (AIST), Tsukuba, Ibaraki, 305-8568, Japan*

[2]*School of Electrical Engineering and Computer Science, Oregon State University, Corvallis, Oregon 97331, USA*

(Received 25 March 2020; revised manuscript received 25 May 2020; accepted 8 June 2020; published 23 June 2020)

It is shown that a surface acoustic wave (SAW) can induce spin resonance of a spin accumulation in a paramagnetic material. The high-frequency mechanical motion of the SAW produces an effective AC magnetic field. If it is oriented orthogonal to the spins, spin precession is induced if an additional DC magnetic field $\mathbf{B}_0$ is applied along the spin axis and the corresponding Larmor frequency ω_0 matches the SAW frequency. The spin accumulation is then resonantly suppressed. We describe this SAW-induced spin resonance quantitatively and analyze the example of a nonlocal spin-transport device with a silicon channel, in which the spin accumulation is created by electrical spin injection from a ferromagnetic contact. The analysis demonstrates that the (nonlocal) electrical detection of SAW-induced spin resonance is feasible.

DOI: 10.1103/PhysRevB.101.214438

I. INTRODUCTION

The manipulation of spin angular momentum is an indispensable aspect of the operation of many spin-based electronic devices [1–5]. Besides the application of an external magnetic field, several new ways to manipulate spins have been developed, including the application of electric fields [6,7], thermal gradients [8–11], magnetic exchange fields [12–14], and spin torques created by spin-polarized currents [15–18]. The efforts to develop methods for the manipulation of conduction electron spins have provided a wealth of knowledge about the interaction of spins with their environment. Interestingly, there has also been a keen interest to explore the coupling between spin and mechanical motion [19–25]. The underlying physical concept is that of spin-rotation coupling, which was revealed in the seminal experiments by Einstein and de Haas [26] and by Barnett [27,28]. Spin-rotation coupling for electrons is described the following Hamiltonian:

$$H_{\mathrm{rot}} = -\mathbf{S} \cdot \boldsymbol{\Omega}_{\mathrm{rot}} \tag{1}$$

with $\mathbf{S}$ the electron spin angular momentum and $\boldsymbol{\Omega}_{\mathrm{rot}}$ the angular velocity of the mechanical rotation. This is equivalent to an effective Zeeman coupling $H_{\mathrm{eff}} = -\gamma\, \mathbf{S} \cdot \mathbf{B}_\Omega$ with an effective magnetic field $\mathbf{B}_\Omega = \boldsymbol{\Omega}_{\mathrm{rot}}/\gamma$, denoted as the Barnett field, in which $\gamma = g\mu_B/\hbar$ is the electron gyromagnetic ratio ($\approx$175.9 GHz/T), μ_B is the Bohr magneton, g is the electron g factor, and $\hbar$ is the reduced Planck's constant.

For the mechanical rotation of an entire object, the angular frequency is typically limited to the kilohertz (kHz) regime, so that the effect on electrons is very small. Also, the integration of the rotation assembly into a spintronic device is rather problematic. Hence our interest is in producing the mechanical motion using a surface acoustic wave (SAW). In solids, surface acoustic waves with frequencies in the range of 100 MHz up to 10 GHz or so can readily be generated by a microwave-driven interdigital transducer (IDT), consisting of two interlocking comb-shaped arrays of metallic electrodes that can be patterned onto the surface of the sample. Continuously driving the IDT causes a periodic displacement of the surface atoms which propagates through the material at the sound velocity. Owing to spin-rotation coupling, this produces [21,23,29–31] an effective AC magnetic field that is oriented parallel to the surface plane and perpendicular to the propagation direction of the SAW and oscillates at the frequency f_{ac} of the SAW. The amplitude B_Ω of the AC Barnett field is given by [23,30,31]

$$B_\Omega = \frac{\omega_{\mathrm{ac}}^2\, u_0}{\gamma\, c}\, \xi^2 \tag{2}$$

with $\omega_{\mathrm{ac}} = 2\pi f_{\mathrm{ac}}$, u_0 the vertical displacement amplitude [30] of the SAW, c the velocity of the SAW, and the dimensionless factor ξ is near unity ($0.87 \leqslant \xi \leqslant 1$, depending on the Poisson ratio [29]). The Barnett field is of the order of several Oe for a SAW with a frequency in the GHz range (Fig. 1). Although B_Ω is not very large, the manipulation of conduction electron spins in a paramagnetic material via Hanle spin precession requires [1] a magnetic field for which the Larmor frequency is of the order of $1/\tau_s$, with τ_s the spin-relaxation time. The spin lifetime of conduction electrons can be of the order of 1–10 ns in semiconductors (such as silicon), metals and two-dimensional materials (such as graphene), which puts the required magnetic fields in the range of several Oe. In spin-transport devices with such materials, it has also been shown that a large spin accumulation (spin splitting of the electrochemical potential) in the range of 1–10 meV can be induced by spin injection from a ferromagnetic (tunnel) contact using an electrical current [32–36]. This makes spin-transport devices a suitable platform to explore the interaction between a spin accumulation and a surface acoustic wave.

Here it is shown that a surface acoustic wave can induce spin resonance of a spin accumulation in a nonmagnetic material. We provide a quantitative description of SAW-induced spin resonance, which can be used to guide the design of

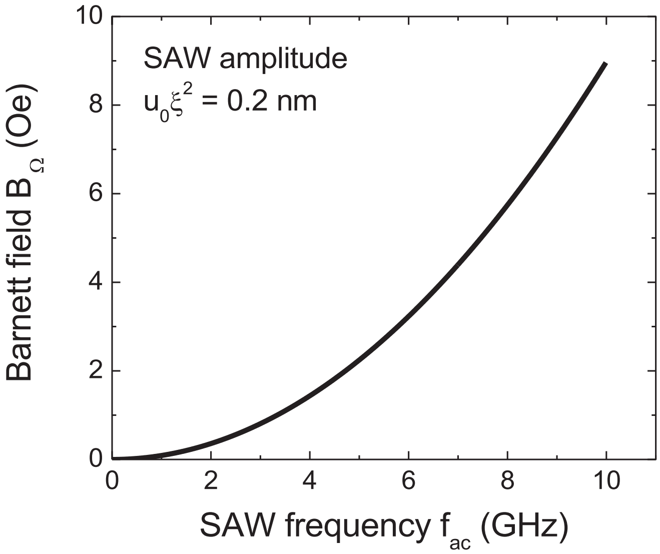

FIG. 1. Magnitude of the AC Barnett field as a function of the frequency of the SAW, for a constant amplitude of the SAW of $u_0\xi^2 = 0.2$ nm, and a wave velocity of 5000 m/s.

experiments and for the interpretation and the quantitative analysis of the data. We describe the specific example of a nonlocal spin-transport device with an *n*-type silicon channel, in which the spin accumulation is created by electrical spin injection from a ferromagnetic contact, and show that the (nonlocal) electrical detection of SAW-induced spin resonance is feasible.

Note that different types of acoustic spin resonance have been discussed and observed in other systems [37–40]. In Ref. [37], it was discussed that the motion of charged ions in insulating crystals produces an oscillating electric field, which couples to the spins and produces a resonant absorption of acoustic power by inducing transitions between the different spin levels. This was indeed observed using bulk crystals subjected to ultrasonic waves [38,39]. More recently, it was shown that the oscillating strain field from a SAW couples to atomic-scale spin centers in silicon carbide [40].

II. RESULTS

A. Description of the system

We shall analyze how a SAW modifies the spin accumulation in the paramagnetic channel of a nonlocal spin-transport device (Fig. 2). The device contains two ferromagnetic (FM) contacts, one for the electrical injection of a spin accumulation into the channel, and the second contact to electrically detect the spins after transport through the channel in the y direction. Two additional nonmagnetic (NM) contacts at the far ends of the device are needed for the application of the current (I) and the detection of the nonlocal voltage (V_{NL}). An interdigital transducer is patterned onto the surface of the channel and driven at GHz frequency. This produces surface acoustic waves that propagate through the channel along the x axis, thus interacting with the spin accumulation between the FM injector and detector. The effective magnetic field $\mathbf{B}_\Omega$ created by the SAW is oriented along the y axis

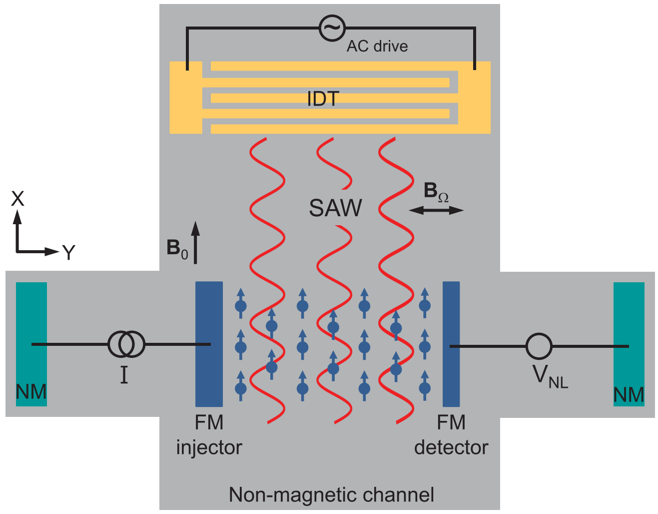

FIG. 2. Device layout for the observation of SAW-induced spin resonance of a spin accumulation. The nonlocal spin-transport device consists of a nonmagnetic channel with four electrical contacts. The two FM contacts serve as injector and detector of the spins in the channel, whereas the two additional nonmagnetic (NM) contacts at the far ends of the device are needed for the application of a current I and the detection of the nonlocal voltage V_{NL}. The IDT, which is patterned onto the surface of the channel, is driven at a microwave frequency, thus producing surface acoustic waves (red wavy lines) that propagate through the channel and interact with the spins (dark blue arrows) between the two FM contacts. The relative dimensions in the x and y directions are not to scale, as the FM contacts typically have aspect ratios larger than 10.

and oscillates at the driving frequency of the IDT. In order to obtain SAW-induced spin resonance, an additional DC magnetic field $\mathbf{B}_0$ is applied along the x direction, which also forces the magnetization of the FM contacts to align along the x direction. Consequently, the spins that are injected into channel are also oriented along x direction. The thickness of the paramagnetic channel is assumed to be small compared to the spin-diffusion length (as in typical nonlocal devices [32–36]), so that the spin accumulation is homogeneous in the depth direction. Moreover, the channel thickness is assumed to be small compared to the wavelength of the SAW (typically $\sim$1 μm for GHz frequencies), so that the atomic displacement amplitude can also be considered as homogenous in the depth direction. Because the FM contacts are typically elongated along the x direction with aspect ratios larger than 10, the spin transport in the channel can be considered as one-dimensional (spin-diffusion along the y direction). Small corrections that account for spin diffusion in the orthogonal direction have been described before [36].

B. Spin dynamics

The spin density $\mathbf{S}$ in the channel of a nonlocal device is obtained from the spin-diffusion equation [1,2] for spin dynamics of an ensemble of spins in a paramagnetic host:

$$\frac{\partial \mathbf{S}}{\partial t} = \mathbf{S} \times \omega_L + D\nabla^2\mathbf{S} - \frac{\mathbf{S}}{\tau_s} \tag{3}$$

with D the diffusion constant, τ_s the spin-relaxation time and $\omega_L = (\omega_x, \omega_y, \omega_z) = \gamma\,(B_x, B_y, B_z)$ the Larmor frequency. The components B_i of the magnetic field contain all the (real and effective) magnetic fields. The terms on the right-hand side of Eq. (3) describe, respectively, spin precession, spin diffusion, and spin relaxation. Spin drift has been neglected. We shall consider the usual case of one-dimensional diffusion (in the lateral y direction only). In general, $\mathbf{S}$ is a vector, but we shall describe the case where the spins injected from the FM injector contact are initially polarized along the x direction, and the FM detector senses the x component of the spin accumulation. We are thus only interested in the x component of the spin accumulation $\Delta\mu$ in the nonmagnetic channel, which is given by [34,36]

$$\Delta\mu(y) = 2e\,J\,P_{\rm inj}\,r_{\rm ch} \int_{-W_{\rm inj}}^{0} \int_{0}^{\infty} S_x(t) \frac{1}{\sqrt{4\pi Dt}} \times \exp\left(-\frac{(y-y_1)^2}{4Dt}\right) \frac{1}{\tau_s} \exp\left(-\frac{t}{\tau_s}\right) dt\,dy_1 \quad (4)$$

with J the injected current density, $P_{\rm inj}$ is the spin polarization of the injected current, e is the electron charge, and $r_{\rm ch}$ is the spin resistance of the channel material [41,42]. The integration over time t and the width $W_{\rm inj}$ of the injector contact in the y direction yields the spin accumulation at location y in the channel produced by spins injected from the injector contact located between $y = -W_{\rm inj}$ and $y = 0$.

The complete integrand of Eq. (4) is the x component of the (normalized) spin density in the channel [solution of Eq. (3)]. Because the terms due to spin diffusion and spin relaxation can be factored out, they are already given explicitly in the integrand. However, we still need to find the spin precession term $S_x(t)$. This is to be obtained from the expression for spin dynamics without the spin diffusion and spin relaxation terms:

$$\frac{\partial \mathbf{S}}{\partial t} = \mathbf{S} \times \omega_L. \quad (5)$$

When there is only an external DC magnetic field along the z direction, perpendicular to the spins, one obtains the usual term $S_x(t) = \cos(\omega_z t)$ that describes the familiar Hanle spin precession. Here we will examine the effect of the AC Barnett field on the spin dynamics. The mathematical analysis has some similarities with that presented by Roundy *et al.* [43], who evaluated Hanle spin precession with an AC drive field, although the system and the specific conditions that we consider here are different.

1. Hanle effect with added AC magnetic field

It is instructive to first consider how the Hanle spin precession in a DC magnetic field B_z perpendicular to the spins is affected by an AC Barnett field, oriented perpendicular to the spins and to the external field. We set

$$\begin{aligned} \omega_x &= 0, \\ \omega_y &= \omega_1 \cos(\omega_{\rm ac} t + \varphi), \\ \omega_z &= \omega_z \end{aligned} \quad (6)$$

with $\omega_z = \gamma\,B_z$ and $\omega_1 = \gamma B_\Omega$. Note that a random phase φ is included [43] to account for the fact that electron spins are injected into the channel at random times (the injection is not synchronized with the AC field). The solution of Eq. (5), after averaging over φ, is then (see Appendix A):

$$S_x(t) = \cos(J_0(\omega_1/\omega_{\rm ac})\,\omega_z t) + \frac{1}{2}\left(\frac{\omega_1}{\omega_{\rm ac}}\right)^2 \cos(\omega_{\rm ac} t) \quad (7)$$

with J_0 the zero-order Bessel function. Because $\omega_1/\omega_{\rm ac}$ is typically of the order of 10^{-4} for the AC field produced by a SAW, we have $J_0(\omega_1/\omega_{\rm ac}) \approx 1$, and also the last term in Eq. (7) can be neglected. The final solution, $S_x(t) \approx \cos(\omega_z t)$, is then identical to the one without the AC field, i.e., the Barnett field has no effect on the Hanle spin precession. This can be understood in the following way. During half of the AC period B_Ω points in one direction, making the spins precess in one direction, while for the other half of the AC cycle, the spins precess back in the opposite way. The maximum angle that the spins can reach is given by the precession rate ($\propto\omega_1$) times the duration of half an AC cycle ($\propto 1/\omega_{\rm ac}$). Because $\omega_1 \ll \omega_{\rm ac}$, the maximum angle is very small. In other words, before any significant precession is made, the AC field reverses sign again and so does the direction of precession.

2. SAW-induced spin resonance

Although the maximum precession angle produced by the AC magnetic field during half a cycle is negligibly small, a strong effect on the spin accumulation is nevertheless achieved when the AC magnetic field is accompanied by a DC magnetic field B_0 aligned *parallel* to the spins, so as to obtain spin resonance. The analysis is more straightforward for a rotating AC field (see Appendix B), however, a SAW produces an effective AC magnetic field that oscillates in amplitude along a fixed axis [21,30]. We thus set

$$\begin{aligned} \omega_x &= \omega_0, \\ \omega_y &= \omega_1 \cos(\omega_{\rm ac} t + \varphi), \\ \omega_z &= 0 \end{aligned} \quad (8)$$

with $\omega_0 = \gamma\,B_0$ and $\omega_1 = \gamma B_\Omega$. The solution for the spin density is then (see Appendix B):

$$S_x(t) = \frac{(\omega_0 - \omega_{\rm ac})^2 + (\omega_1/2)^2 \cos(\Omega_L t)}{(\omega_0 - \omega_{\rm ac})^2 + (\omega_1/2)^2}. \quad (9)$$

with the effective Larmor frequency

$$\Omega_L = \sqrt{(\omega_0 - \omega_{\rm ac})^2 + (\omega_1/2)^2}. \quad (10)$$

When the DC field is far from the resonance value ($(\omega_0 - \omega_{\rm ac})^2 \gg (\omega_1/2)^2$), the spin density is constant ($S_x(t) = 1$), and there is no spin precession. However, at resonance, when $B_0 = \omega_{\rm ac}/\gamma$, we have $S_x(t) = \cos((\omega_1/2)t)$. At resonance, the combined effect of the AC and DC fields is equivalent to spin precession at a Larmor frequency $\omega_1/2 = \gamma B_\Omega/2$, and thus the spin density is reduced by an amount that depends on the amplitude of the AC field.

Let us illustrate the effect of the SAW on the spin accumulation in the absence of spin diffusion, which yields the following expression for the spin accumulation:

$$\Delta\mu \propto \left[\frac{(\omega_0-\omega_{ac})^2}{(\omega_0-\omega_{ac})^2+(\omega_1/2)^2}+\left(\frac{(\omega_1/2)^2}{(\omega_0-\omega_{ac})^2+(\omega_1/2)^2}\right)\left(\frac{1}{1+(\Omega_L\,\tau_s)^2}\right)\right]. \tag{11}$$

Figure 3 displays the calculated spin accumulation in the presence of SAW-induced spin resonance. Close to resonance ($\gamma\,B_0 \approx 2\,\pi\,f_{ac}$) the spin accumulation is significantly suppressed, and the suppression becomes stronger at larger SAW frequency, because the AC Barnett field increases with f_{ac}. Importantly, the width of the SAW-induced spin-resonance line is determined both by τ_s and by ω_1, as can be deduced from Eq. (11).

In the next section, we shall analyze the detection of the SAW-induced spin resonance for a nonlocal spin-transport device, including spin diffusion. This requires [34] numerical evaluation of Eq. (4), because the result depends on the geometrical parameters of the device (widths of the FM injector and detector contacts and their separation).

C. SAW-induced spin resonance in a silicon nonlocal device

We evaluate the spin signal produced by SAW-induced spin resonance in a nonlocal spin-transport device with a Si channel, using parameters previously established from nonlocal spin-transport data [34–36] ($\tau_s = 18$ ns, spin-diffusion length 2.2 μm). We assume that the width of the FM injector in the y direction is 1 μm, and calculate the spin accumulation at the center of the nonlocal detector contact by numerical evaluation of Eq. (4) with Eq. (9) for $S_x(t)$, for different distances d between the detector center and the edge of the injector (Fig. 4, left panel). The SAW has a frequency of 10 GHz and the external field B_0 is parallel to the spins.

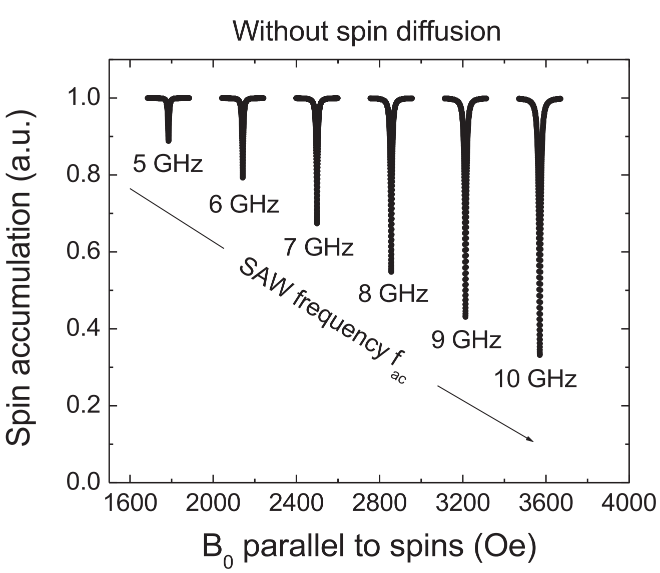

FIG. 3. SAW-induced spin resonance without spin diffusion. The spin accumulation as a function of the external magnetic field B_0 parallel to the spins was calculated in the absence of spin diffusion [Eq. (11)], for different values of the frequency f_{ac} of the SAW, as indicated. Other parameters: $u_0\xi^2 = 0.2$ nm, $c = 5000$ m/s, and $\tau_s = 18$ ns.

When B_0 is swept through the resonance, a sharp reduction of the nonlocal spin signal occurs. For a distance of 1 μm, the spin signal is reduced by about a factor of 2. At larger d, the relative dip in the signal becomes stronger, and a complete suppression of the spin accumulation is obtained at resonance. The dependence on d is because for larger distances the electron spins have more time to precess before reaching the detector, thus producing a larger precession angle. Thus the SAW-induced spin resonance becomes more pronounced at larger separation between injector and nonlocal detector. The right panel of Fig. 4 shows how the nonlocal spin signal at resonance ($B_0 = 3572.4$ Oe for $f_{ac} = 10$ GHz) decays as a function of the amplitude of the SAW. For small distance, the complete suppression of the spin signal requires a SAW amplitude above 0.4 nm, which is difficult to achieve experimentally. However, SAW amplitudes of 0.1 to 0.2 nm are sufficient for distances of 4 μm and above.

III. DISCUSSION

For a nonlocal device with a given set of geometric parameters, the width of the SAW-induced spin resonance line depends on B_Ω and on τ_s. If the magnitude of the Barnett field is known, one can determine the spin lifetime from the SAW spin-resonance line width. However, in a nonlocal device the spin accumulation is created by electrical injection, and thus τ_s can readily be obtained [32–36] by applying only a DC field perpendicular to the spins (regular Hanle measurement), without the need for the AC field produced by the SAW. With τ_s known, one can thus determine the Barnett field from the line width of SAW-induced spin resonance. Note the essential difference with conventional electron spin resonance (ESR) in paramagnetic materials [44], in which the DC field is needed to create a net spin polarization and spin precession cannot be induced with an additional DC field perpendicular to the spins (this would just reorient the spin polarization). That is, in conventional ESR one needs the resonance produced by an AC field in order to determine the spin lifetime.

Although the analysis was performed for a nonlocal device, the SAW-induced spin resonance can occur in any device in which there exists a spin accumulation, created electrically, optically or thermally. In two-terminal lateral spin-transport devices, the analysis of SAW-induced spin resonance requires more effort, because the Hanle spin signal consists of a superposition of four contributions [45]. Nevertheless, the analysis is straightforward since the description of each of the four contributions is similar to that of a nonlocal Hanle signal, as recently shown [45]. In devices with the three-terminal geometry [46], the SAW-induced spin resonance can also be observed, but the magnitude of the resonance peak is reduced, because the effective distance between the point of injection and detection is smaller than in a nonlocal device (recall that the effect of the SAW is reduced at smaller distance between injector and detector, as shown above).

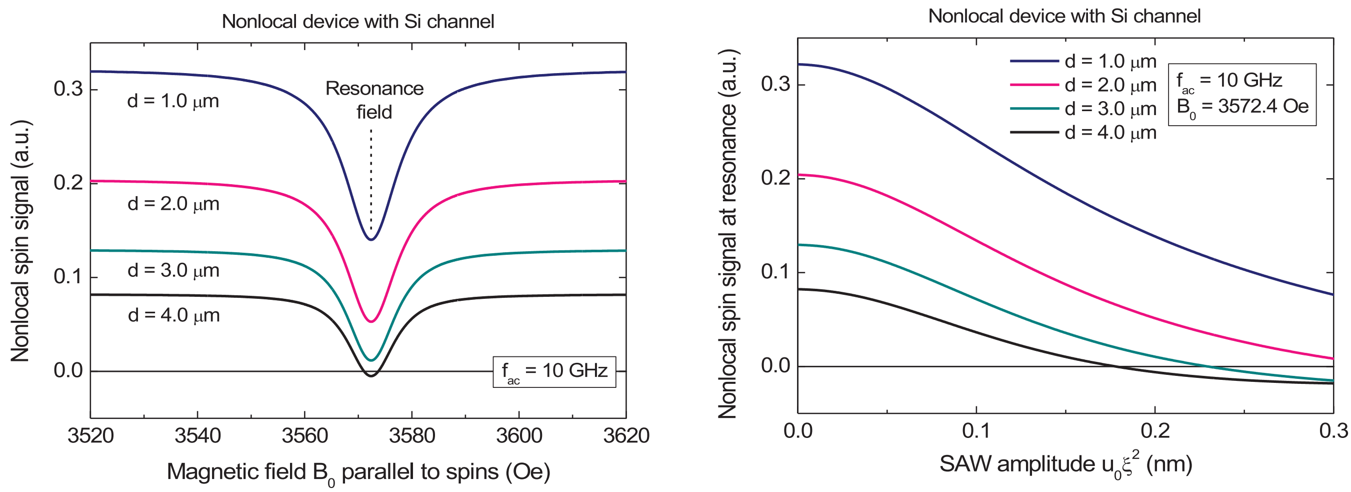

FIG. 4. SAW-induced spin resonance in a nonlocal spin-transport device. Left panel: spin signal as a function of the external magnetic field B_0 parallel to the spins, calculated for a nonlocal device with a Si channel ($\tau_s = 18$ ns, spin-diffusion length 2.2 μm) and a 1 μm wide FM injector contact, for different distances d between the edge of the injector and the center of the nonlocal detector contact, as indicated. Parameters of the SAW: $f_{\mathrm{ac}} = 10$ GHz, $u_0\xi^2 = 0.2$ nm, and $c = 5000$ m/s. Right panel: nonlocal spin signal at resonance ($B_0 = 3572.4$ Oe) as a function of the amplitude u_0 of the SAW, at different distances d between injector and detector ($f_{\mathrm{ac}} = 10$ GHz and $c = 5000$ m/s).

In our description, the SAW produces an effective AC magnetic field that modifies spin precession and produces spin resonance. However, any effect of the SAW on the spin lifetime was neglected. In reality, the SAW produces a time-varying strain, and it is known that in semiconductors, the spin lifetime changes under the application of strain [47–49]. One may therefore expect that in the presence of a SAW, the spin lifetime oscillates at the SAW frequency. A refined description of SAW-induced spin resonance should take this into account, for instance by including an effective spin lifetime obtained by averaging the time-dependent spin lifetime over a period of the fast AC oscillation [note that the AC period is of the order of 0.1 ns, and thus much smaller than the spin lifetime ($\sim$10 ns)]. This is not a simple exercise, because (i) the magnitude and direction of the strain produced by a SAW is inhomogeneous in space, (ii) the spins in the channel material are moving by diffusion, and (iii), the precise relation between strain and spin lifetime needs to be known. So far, we have only made a rough estimate, which indicates that for the calculations presented in this manuscript, the effect of the SAW on the spin lifetime is minimal [50]. Fortunately, in the nonlocal spin-transport devices considered here, the effect of the SAW on the spin lifetime can be measured directly, namely, by performing a regular Hanle measurement in small perpendicular DC magnetic fields (far from any resonance), with and without the SAW.

IV. SUMMARY

It was shown that a surface acoustic wave can induce spin resonance of a spin accumulation in a nonmagnetic material. A quantitative description of SAW-induced spin resonance was presented and the conditions for it to occur were obtained. This can be used to guide and interpret experiments and to analyze the data. The SAW-induced spin resonance was evaluated for a nonlocal spin-transport device with a silicon channel, in which the spin accumulation is created by electrical spin injection from a ferromagnetic contact. The analysis demonstrates that the (nonlocal) electrical detection of SAW-induced spin resonance is feasible.

ACKNOWLEDGMENT

This work was supported by the JSPS Invitational Fellowship for Research in Japan of P.D. (Grant No. S19035).

APPENDIX A

In this Appendix, we evaluate the expression for $S_x(t)$ for the case of Hanle spin precession in a DC magnetic field perpendicular to the spins, with an additional AC magnetic field, also oriented perpendicular to the spins. We thus seek the solution of the spin-dynamics equation $\partial\mathbf{S}/\partial\mathbf{t} = \mathbf{S} \times \omega_{\mathbf{L}}$ for

$$\begin{aligned} \omega_x &= 0, \\ \omega_y &= \omega_1 \cos(\omega_{\mathrm{ac}} t + \varphi), \\ \omega_z &= \omega_z \end{aligned} \tag{A1}$$

with $\omega_z = \gamma B_z$, whereas $\omega_1 = \gamma B_\Omega$ for an AC field generated by a SAW. It is convenient [43] to change variables:

$$\begin{aligned} x' &= x \cos(\theta(t)) - z \sin(\theta(t)), \\ y' &= y, \quad z' = x \sin(\theta(t)) + z \cos(\theta(t)) \end{aligned} \tag{A2}$$

with $\theta(t) = (\omega_1/\omega_{\mathrm{ac}}) \sin(\omega_{\mathrm{ac}} t + \varphi)$. The spin-dynamics equations then transform into:

$$\begin{aligned} \frac{\partial S_x'}{\partial t} &= S_y' [\omega_z \cos(\theta(t))] - S_z' [2\omega_1 \cos(\omega_{\mathrm{ac}} t + \varphi)], \\ \frac{\partial S_y'}{\partial t} &= S_z' [-\omega_z \sin(\theta(t))] - S_x' [\omega_z \cos(\theta(t))], \\ \frac{\partial S_z'}{\partial t} &= S_x' [2\omega_1 \cos(\omega_{\mathrm{ac}} t + \varphi)] - S_y' [-\omega_z \sin(\theta(t))] \end{aligned} \tag{A3}$$

implying that after transformation $\omega'_x = -\omega_z \sin(\theta(t))$, $\omega'_y = 2\,\omega_1 \cos(\omega_{ac} t + \varphi)$ and $\omega'_z = \omega_z \cos(\theta(t))$. Also, the initial conditions $[S_x(0) = 1, S_y(0) = S_z(0) = 0]$ transform into $S'_x(0) = \cos((\omega_1/\omega_{ac}) \sin\varphi)$, $S'_y(0) = 0$, and $S'_z(0) = \sin((\omega_1/\omega_{ac}) \sin\varphi)$ in the new coordinate frame. Because ω_{ac} is much larger than any of the Larmor frequencies, the equations can be averaged [43] over a period of the fast AC dynamics, noting that

$$\begin{aligned} \int_{-\pi/\omega_{ac}}^{+\pi/\omega_{ac}} \cos(\theta(t))dt &= J_0(\omega_1/\omega_{ac}), \\ \int_{-\pi/\omega_{ac}}^{+\pi/\omega_{ac}} \sin(\theta(t))dt &= 0, \\ \int_{-\pi/\omega_{ac}}^{+\pi/\omega_{ac}} \cos(\omega_{ac} t + \varphi)dt &= 0 \end{aligned} \tag{A4}$$

with J_0 the zero-order Bessel function. After averaging we then have

$$\begin{aligned} \frac{\partial S'_x}{\partial t} &= S'_y\, \omega_z\, J_0(\omega_1/\omega_{ac}), \\ \frac{\partial S'_y}{\partial t} &= -S'_x\, \omega_z\, J_0(\omega_1/\omega_{ac}), \\ \frac{\partial S'_z}{\partial t} &= 0. \end{aligned} \tag{A5}$$

Because the effective field components are now independent of time, we can use the general solution presented in Appendix C. Applying the above-mentioned initial conditions, the solutions are

$$\begin{aligned} S'_x(t) &= \cos((\omega_1/\omega_{ac}) \sin\varphi)\, \cos(J_0(\omega_1/\omega_{ac})\, \omega_z\, t), \\ S'_y(t) &= -\cos((\omega_1/\omega_{ac}) \sin\varphi)\, \sin(J_0(\omega_1/\omega_{ac})\, \omega_z\, t), \\ S'_z(t) &= \sin((\omega_1/\omega_{ac}) \sin\varphi). \end{aligned} \tag{A6}$$

Finally, after transforming back to the (x, y, z) coordinate system and averaging over the initial phase φ, we obtain for the x component:

$$S_x(t) = \cos(J_0(\omega_1/\omega_{ac})\, \omega_z\, t) + \frac{1}{2}\left(\frac{\omega_1}{\omega_{ac}}\right)^2 \cos(\omega_{ac}\, t). \tag{A7}$$

APPENDIX B

In this Appendix, we present the solution of the spin-dynamics equation $\partial\mathbf{S}/\partial\mathbf{t} = \mathbf{S} \times \omega_\mathbf{L}$ with a DC magnetic field *parallel* to the spins and an AC field perpendicular to the spins, which yields spin resonance. It is convenient to first change to a rotating coordinate system (x', y', z'), with $x' = x$, $y' = y \cos(\omega_{ac} t) - z \sin(\omega_{ac} t)$ and $z' = z \cos(\omega_{ac} t) + y \sin(\omega_{ac} t)$. The spin-dynamics equation then changes to $\partial\mathbf{S}'/\partial\mathbf{t} = \mathbf{S}' \times \omega'_\mathbf{L}$, with an effective field characterized by

$$\begin{aligned} \omega'_x &= \omega_x - \omega_{ac}, \\ \omega'_y &= \omega_y \cos(\omega_{ac} t) - \omega_z \sin(\omega_{ac} t), \\ \omega'_z &= \omega_z \cos(\omega_{ac} t) + \omega_y \sin(\omega_{ac} t). \end{aligned} \tag{B1}$$

Let us first consider a *rotating* AC field with amplitude ω_1:

$$\begin{aligned} \omega_x &= \omega_0, \\ \omega_y &= +\omega_1 \cos(\omega_{ac} t + \varphi), \\ \omega_z &= -\omega_1 \sin(\omega_{ac} t + \varphi). \end{aligned} \tag{B2}$$

The effective fields in the rotating frame are then

$$\begin{aligned} \omega'_x &= \omega_0 - \omega_{ac}, \\ \omega'_y &= +\omega_1 \cos(\varphi), \\ \omega'_z &= -\omega_1 \sin(\varphi). \end{aligned} \tag{B3}$$

Because the effective fields in the rotating frame do not depend on time, we can use the general solution of the spin-dynamics equation (Appendix C), noting that the initial conditions at $t = 0$ $[S_x(0) = 1, S_y(0) = S_z(0) = 0]$ transform into $S'_x(0) = 1, S'_y(0) = S'_z(0) = 0$ in the rotating frame. The solution for the x component of the spin density $S_x(t)$ in the laboratory frame is then

$$S_x(t) = S'_x(t) = \frac{\omega'^2_x + \left(\omega'^2_y + \omega'^2_z\right) cos(\omega'_L\, t)}{\omega'^2_L} \tag{B4}$$

with ${\omega'_L}^2 = \omega'^2_x + \omega'^2_y + \omega'^2_z$. We thus have

$$S_x(t) = \frac{(\omega_0 - \omega_{ac})^2 + (\omega_1)^2 \cos(\Omega_L\, t)}{(\omega_0 - \omega_{ac})^2 + (\omega_1)^2}. \tag{B5}$$

with

$$\Omega_L = \sqrt{(\omega_0 - \omega_{ac})^2 + (\omega_1)^2}. \tag{B6}$$

Note that the solution does not depend on the initial phase φ, so that the averaging over φ is unnecessary. Also note that if a rotating AC field with the opposite sense of rotation is used, the solution is similar, but the factor $\omega_0 - \omega_{ac}$ changes to $\omega_0 + \omega_{ac}$, so that no spin resonance is produced at positive magnetic fields ($\omega_0 > 0$).

Next, we consider an *oscillating* AC field with amplitude ω_1:

$$\begin{aligned} \omega_x &= \omega_0, \\ \omega_y &= \omega_1 \cos(\omega_{ac} t + \varphi), \\ \omega_z &= 0. \end{aligned} \tag{B7}$$

This yields the following effective fields in the rotating frame:

$$\begin{aligned} \omega'_x &= \omega_0 - \omega_{ac}, \\ \omega'_y &= \omega_1 \cos(\omega_{ac} t) \cos(\omega_{ac} t + \varphi), \\ \omega'_z &= \omega_1 \sin(\omega_{ac} t) \cos(\omega_{ac} t + \varphi). \end{aligned} \tag{B8}$$

As may have been expected, for an oscillating AC field, the transformation to the rotating coordinate frame does not yield effective fields that are time-independent. Hence, an additional step is required, namely, the averaging of the spin-dynamics equation in the rotating frame over a period of the fast AC dynamics (similar to what was done in Appendix A).

Noting that

$$\int_{-\pi/\omega_{\rm ac}}^{+\pi/\omega_{\rm ac}} \omega_y' dt = +\frac{1}{2}\,\omega_1\,\cos(\varphi),$$
$$\int_{-\pi/\omega_{\rm ac}}^{+\pi/\omega_{\rm ac}} \omega_z' dt = -\frac{1}{2}\,\omega_1\,\sin(\varphi), \tag{B9}$$

we obtain after averaging over the fast AC dynamics:

$$\begin{aligned} \omega_x' &= \omega_0 - \omega_{\rm ac}, \\ \omega_y' &= +(\omega_1/2)\,\cos(\varphi), \\ \omega_z' &= -(\omega_1/2)\,\sin(\varphi). \end{aligned} \tag{B10}$$

The effective fields are now independent of time, and in fact, they are identical to those for the rotating AC field, except that ω_1 is replaced by $\omega_1/2$. The solution for the spin density is thus:

$$S_x(t) = \frac{(\omega_0 - \omega_{\rm ac})^2 + (\omega_1/2)^2\cos(\Omega_L\,t)}{(\omega_0 - \omega_{\rm ac})^2 + (\omega_1/2)^2} \tag{B11}$$

with

$$\Omega_L = \sqrt{(\omega_0 - \omega_{\rm ac})^2 + (\omega_1/2)^2}. \tag{B12}$$

Note that the appearance of the factor of (1/2) is well known from conventional electron spin resonance [44]. It can be understood as follows. An oscillating AC field with amplitude ω_1 can be decomposed into a sum of two rotating AC fields with opposite sense of rotation and half the amplitude. As noted above, at positive magnetic fields spin resonance occurs only for one sense of rotation, while for the oppositely rotating field, the system is far from resonance and there is little effect on the spins. One can thus retain only the rotating field that produces spin resonance, and replace the amplitude ω_1 by $\omega_1/2$.

APPENDIX C

In this Appendix, we present the general solution of the spin-dynamics equation $\partial\mathbf{S}/\partial\mathbf{t} = \mathbf{S}\times\boldsymbol{\omega}_{\mathbf{L}}$ for arbitrary initial conditions:

$$\begin{aligned} S_x(t=0) &= A, \\ S_y(t=0) &= B, \\ S_z(t=0) &= C \end{aligned} \tag{C1}$$

with A, B, C constants subject to the condition $A^2 + B^2 + C^2 = 1$ for a normalized spin density. Although the solution for initial conditions $A = 1$ and $B = C = 0$ is often used [51], the general solution is required if after transformation to a different coordinate system, B and C are no longer zero (as, for instance, in Appendix A). Provided that all the components of the magnetic field are *independent of time*, the general solution has the form:

$$\begin{aligned} S_x(t) &= [C_1\,\cos(\omega_L\,t) + C_2\,\sin(\omega_L\,t) + C_3]/\omega_L^2, \\ S_y(t) &= [C_4\,\cos(\omega_L\,t) + C_5\,\sin(\omega_L\,t) + C_6]/\omega_L^2, \\ S_z(t) &= [C_7\,\cos(\omega_L\,t) + C_8\,\sin(\omega_L\,t) + C_9]/\omega_L^2 \end{aligned} \tag{C2}$$

with the constants C_1 to C_9 given by

$$\begin{aligned} C_1 &= A\left(\omega_y^2 + \omega_z^2\right) - B\,\omega_x\omega_y - C\,\omega_x\omega_z, \\ C_2 &= B\,\omega_z\omega_L - C\,\omega_y\omega_L, \\ C_3 &= A\,\omega_x^2 + B\,\omega_x\omega_y + C\,\omega_x\omega_z, \\ C_4 &= -A\,\omega_x\omega_y + B\left(\omega_x^2 + \omega_z^2\right) - C\,\omega_y\omega_z, \\ C_5 &= -A\,\omega_z\omega_L + C\,\omega_x\omega_L, \\ C_6 &= A\,\omega_x\omega_y + B\,\omega_y^2 + C\,\omega_y\omega_z, \\ C_7 &= -A\,\omega_x\omega_z - B\,\omega_y\omega_z + C\left(\omega_x^2 + \omega_y^2\right), \\ C_8 &= A\,\omega_y\omega_L - B\,\omega_x\omega_L, \\ C_9 &= A\,\omega_x\omega_z + B\,\omega_y\omega_z + C\,\omega_z^2. \end{aligned} \tag{C3}$$

[1] I. Žutić, J. Fabian, and S. Das Sarma, Spintronics: fundamentals and applications, Rev. Mod. Phys. **76**, 323 (2004).

[2] J. Fabian, A. Matos-Abiague, C. Ertler, P. Stano, and I. Žutić, Semiconductor spintronics, Acta Physica Slovaca **57**, 565 (2007).

[3] A. Fert, Nobel Lecture: Origin, development, and future of spintronics, Rev. Mod. Phys. **80**, 1517 (2008).

[4] S. Sugahara and J. Nitta, Spin-transistor electronics: an overview and outlook, Proc. IEEE **98**, 2124 (2010).

[5] R. Jansen, Silicon spintronics, Nat. Mater. **11**, 400 (2012).

[6] J. Nitta, T. Akazaki, H. Takayanagi, and T. Enoki, Gate Control of Spin-Orbit Interaction in an Inverted InGaAs/InAlAs Heterostructure, Phys. Rev. Lett. **78**, 1335 (1997).

[7] H. Ohno, D. Chiba, F. Matsukura, T. Omiya, E. Abe, T. Dietl, Y. Ohno, and K. Ohtani, Electric field control of ferromagnetism, Nature (London) **408**, 944 (2000).

[8] K. Uchida, S. Takahashi, K. Harii, J. Ieda, W. Koshibae, K. Ando, S. Maekawa, and E. Saitoh, Observation of the spin Seebeck effect, Nature (London) **455**, 778 (2008).

[9] A. Slachter, F. L. Bakker, J. P. Adam, and B. J. van Wees, Thermally driven spin injection from a ferromagnet into a nonmagnetic metal, Nat. Phys. **6**, 879 (2010).

[10] J. C. Le Breton, S. Sharma, H. Saito, S. Yuasa, and R. Jansen, Thermal spin current from a ferromagnet to silicon by Seebeck spin tunnelling, Nature (London) **475**, 82 (2011).

[11] G. E. W. Bauer, E. Saitoh, and B. J. van Wees, Spin caloritronics, Nat. Mater. **11**, 391 (2012).

[12] P. Wei, S. Lee, F. Lemaitre, L. Pinel, D. Cutaia, W. Cha, F. Katmis, Y. Zhu, D. Heiman, J. Hone, J. S. Moodera, and C.-T. Chen, Strong interfacial exchange field in the graphene/EuS heterostructure, Nat. Mater. **15**, 711 (2016).

[13] J. Ch. Leutenantsmeyer, A. A. Kaverzin, M. Wojtaszek, and B. J. van Wees, Proximity induced room temperature ferromagnetism in graphene probed with spin currents, 2D Mater. **4**, 014001 (2017).
[14] R. Jansen, A. Spiesser, H. Saito, Y. Fujita, S. Yamada, K. Hamaya, and S. Yuasa, Proximity exchange coupling in a Fe/MgO/Si tunnel contact detected by the inverted Hanle effect, Phys. Rev. B **100**, 174432 (2019).
[15] J. C. Slonczewski, Current-driven excitations of magnetic multilayers, J. Magn. Magn. Mater. **159**, L1 (1996).
[16] S. I. Kiselev, J. C. Sankey, I. N. Krivorotov, N. C. Emley, R. J. Schoelkopf, and R. A. Buhrman, and D. C. Ralph, Microwave oscillations of a nanomagnet driven by a spin-polarized current, Nature (London) **425**, 380 (2003).
[17] A. Deac, A. Fukushima, H. Kubota, H. Maehara, Y. Suzuki, S. Yuasa, Y. Nagamine, K. Tsunekawa, D. D. Djayaprawira, and N. Watanabe, Bias-driven high-power microwave emission from MgO-based tunnel magnetoresistance devices, Nat. Phys. **4**, 803 (2008).
[18] A. Manchon, J. Železný, I. M. Miron, T. Jungwirth, J. Sinova, A. Thiaville, K. Garello, and P. Gambardella, Current-induced spin-orbit torques in ferromagnetic and antiferromagnetic systems, Rev. Mod. Phys. **91**, 035004 (2019).
[19] S. Bretzel, G. E. W. Bauer, Y. Tserkovnyak, and A. Brataas, Barnett effect in thin magnetic films and nanostructures, Appl. Phys. Lett. **95**, 122504 (2009).
[20] H. Chudo, M. Ono, K. Harii, M. Matsuo, J. Ieda, R. Haruki, S. Okayasu, S. Maekawa, H. Yasuoka, and E. Saitoh, Observation of Barnett fields in solids by nuclear magnetic resonance, Appl. Phys. Express **7**, 063004 (2014).
[21] J. Ieda, M. Matsuo, and S. Maekawa, Theory of mechanical spin current generation via spin-rotation coupling, Sol. St. Commun. **198**, 52 (2014).
[22] M. Matsuo, J. Ieda, and S. Maekawa, Mechanical generation of spin current, Front. Phys. **3**, 54 (2015).
[23] E. M. Chudnovsky and R. Jaafar, Manipulating the magnetization of a nanomagnet with surface acoustic waves: spin-rotation mechanism, Phys. Rev. Appl. **5**, 031002 (2016).
[24] M. Matsuo, E. Saitoh, and S. Maekawa, Spin-mechatronics, J. Phys. Soc. Jap. **86**, 011011 (2017).
[25] D. Kobayashi, T. Yoshikawa, M. Matsuo, R. Iguchi, S. Maekawa, E. Saitoh, and Y. Nozaki, Spin Current Generation Using a Surface Acoustic Wave Generated via Spin-Rotation Coupling, Phys. Rev. Lett. **119**, 077202 (2017).
[26] A. Einstein and W. J. de Haas, Experimental proof of the existence of Ampere's molecular currents, Verh. Dtsch. Phys. Ges. **17**, 152 (1915).
[27] S. J. Barnett, Magnetization by rotation, Phys. Rev. **6**, 239 (1915).
[28] S. J. Barnett, Gyromagnetic and electron-inertia effects, Rev. Mod. Phys. **7**, 129 (1935).
[29] L. D. Landau and E. M. Lifshitz, *Theory of Elasticity* (Pergamon Press, Oxford, 1970).
[30] For a Rayleigh wave, the only nonzero component of the rotation tensor corresponds to rotation along the y axis, perpendicular to surface and to the direction of propagation. The AC Barnett field due to spin-rotation coupling is thus linearly polarized along the y axis. Moreover, for the longitudinal part of a Rayleigh wave, the rotation vanishes [29]. The AC Barnett field thus originates from the transverse part of the wave. The parameter u_0 is defined as the vertical displacement amplitude of the transverse part of the SAW.
[31] The Barnett field has a maximum value at the surface [given by Eq. (2)] and decays exponentially as a function of the depth as $\exp(-\kappa_t z)$, with $\kappa_t = k\sqrt{1-\xi^2}$ describing the decay of the transverse part of the SAW, assumed to be a Rayleigh wave [29] with wave number k. For $f_{ac} = 10$ GHz, $c = 5000$ m/s, and $\xi = 0.95$, the Barnett field at a distance of 70 nm from the surface, which is the typical thickness of the Si transport channel in nonlocal devices, is 0.76 of the maximum value. In the calculations of the SAW-induced spin resonance, we have taken the Barnett field to be independent of the depth for convenience, assuming that the transport channel is sufficiently thin.
[32] W. Han, K. Pi, K. M. McCreary, Y. Li, J. J. I. Wong, A. G. Swartz, and R. K. Kawakami, Tunneling Spin Injection into Single Layer Graphene, Phys. Rev. Lett. **105**, 167202 (2010).
[33] M. Gurram, S. Omar, and B. J. van Wees, Bias induced up to 100% spin-injection and detection polarizations in ferromagnet/bilayerhBN/graphene/hBN heterostructures, Nat. Commun. **8**, 248 (2017).
[34] A. Spiesser, H. Saito, Y. Fujita, S. Yamada, K. Hamaya, S. Yuasa, and R. Jansen, Giant Spin Accumulation in Silicon Nonlocal Spin-Transport Devices, Phys. Rev. Appl. **8**, 064023 (2017).
[35] R. Jansen, A. Spiesser, H. Saito, Y. Fujita, S. Yamada, K. Hamaya, and S. Yuasa, Nonlinear Electrical Spin Conversion in a Biased Ferromagnetic Tunnel Contact, Phys. Rev. Appl. **10**, 064050 (2018).
[36] A. Spiesser, H. Saito, S. Yuasa, and R. Jansen, Tunnel spin polarization of Fe/MgO/Si contacts reaching 90% with increasing MgO thickness, Phys. Rev. B **99**, 224427 (2019).
[37] B. I. Kochelaev and Y. V. Yablokov, *The beginning of Paramagnetic Resonance* (World Scientific, Singapore, 1995), p. 100, and references therein.
[38] W. G. Proctor and W. H. Tantilla, Saturation of nuclear electric quadrupole energy levels by ultrasonic excitation, Phys. Rev. **98**, 1854 (1955).
[39] E. H. Jacobsen, N. S. Shiren, and E. B. Tucker, Effects of 9.2-kMc/sec Ultrasonics on Electron Spin Resonances in Quartz, Phys. Rev. Lett. **3**, 81 (1959).
[40] A. Hernández-Mínguez, A. V. Poshakinskiy, M. Hollenbach, P. V. Santos, and G. V. Astakhov, Anisotropic spin-acoustic resonance in silicon carbide at room temperature, arXiv:2005.00787.
[41] A. Fert and H. Jaffrès, Conditions for efficient spin injection from a ferromagnetic metal into a semiconductor, Phys. Rev. B **64**, 184420 (2001).
[42] R. Jansen, S. P. Dash, S. Sharma, and B. C. Min, Silicon spintronics with ferromagnetic tunnel devices, Semicond. Sci. Technol. **27**, 083001 (2012).
[43] R. C. Roundy, M. C. Prestgard, A. Tiwari, and M. E. Raikh, Shape of the Hanle curve in spin-transport structures in the presence of an ac drive, Phys. Rev. B **90**, 205203 (2014).
[44] I. I. Rabi, J. R. Zacharias, S. Millman and P. Kusch, A new method of measuring nuclear magnetic moment, Phys. Rev. **53**, 318 (1938).
[45] A. Spiesser, Y. Fujita, H. Saito, S. Yamada, K. Hamaya, S. Yuasa, and R. Jansen, Hanle spin precession in a two-terminal lateral spin valve, Appl. Phys. Lett. **114**, 242401 (2019).

[46] X. Lou, C. Adelmann, M. Furis, S. A. Crooker, C. J. Palmstrøm, and P. A. Crowell, Electrical Detection of Spin Accumulation at a Ferromagnet-Semiconductor Interface, Phys. Rev. Lett. **96**, 176603 (2006).

[47] Edited by B. P. Zakharchenya, and F. Meyer, *Optical Orientation*, (Elsevier, Amsterdam, 1984).

[48] J.-M. Tang, B. T. Collins and M. E. Flatté, Electron spin-phonon interaction symmetries and tunable spin relaxation in silicon and germanium, Phys. Rev. B **85**, 045202 (2012).

[49] O. Chalaev, Y. Song, and H. Dery, Suppressing the spin relaxation of electrons in silicon, Phys. Rev. B **95**, 035204 (2017).

[50] The peak strain for a SAW with amplitude u_0 is approximately equal to $ku_0 = 2\pi u_0/\lambda$. For $f_{ac} = 10$ GHz and $c = 5000$ m/s, the SAW wavelength $\lambda = 0.5$ μm and the peak strain is 0.0025 for $u_0 = 0.2$ nm as used in the calculations. According to Ref. [52], a strain of 0.0025 translates into a valley splitting of the Si conduction band of about 40 meV. This, in turn, leads to an increase in the spin lifetime in Si, but according to the calculations in Ref. [49], specifically Fig. 4 therein, the increase is very small for Si heavily doped with phosphorous. Based on this, and the fact that during most of the AC cycle the displacement is smaller than the 0.2 nm peak value, the overall effect on the spin lifetime is expected to be weak for the numerical calculations presented in this manuscript.

[51] S. P. Dash, S. Sharma, J. C. Le Breton, J. Peiro, H. Jaffrès, J.-M. George, A. Lemaître, and R. Jansen, Spin precession and inverted Hanle effect in a semiconductor near a finite-roughness ferromagnetic interface, Phys. Rev. B **84**, 054410 (2011).

[52] S. Richard, F. Aniel, G. Fishman, and N. Cavassilas, Energy-band structure in strained silicon: A 20-band k·p and Bir-Pikus Hamiltonian model, J. Appl. Phys. **94**, 1795 (2003).